On the thermomechanics and footprint of fragmenting blasts

T.I. Zohdi [a,*], J. Cabalo [b]

[a] *Department of Mechanical Engineering 6195 Etcheverry Hall, University of California, Berkeley, CA, 94720-1740, USA*
[b] *US Army ECBC, RDCB-DRI-T, 5183 Blackhawk Rd, APG, MD 21010, USA*

ARTICLE INFO

ABSTRACT

In this paper, a mathematical model is developed to simulate the progressive time-evolution of an object that fragments, which may contain biohazardous materials or materials that may thermally degrade into a toxic state. Estimates are made for the blast radius that one can expect for a given amount of detonation energy and the resulting atmospheric heating of fragments. The atmospheric heating of the fragments is important, since if the heating is sufficiently high, the biohazardous material can be neutralized. If the material is not heated sufficiently, then the location in which it lands can be considered as "contaminated". This analysis is useful is determining safe areas after such a blast. Ascertaining the temperature of the fragments is extremely difficult to measure in experiments, thus motivating the development of the model. The model balances the released energy from the initial blast pulse with the subsequent kinetic energy and then numerically computes the trajectory of the fragments under the influence of the drag from the surrounding air and gravity. Preliminary field experiments with explosives are described and the results are compared to the output from the model. The subsequent drag heating of the material is then computed in order to ascertain the temperature of the blast fragments.

Published by Elsevier Ltd.

1. Introduction

Understanding the blast fragmentation of objects that contain biohazardous material has wide-ranging applications, especially with respect to emergency management, and limitation of human exposure. Events involving explosions and biohazardous materials include accidents at chemical production or water treatment facilities that may release clouds of toxic industrial material, or even deliberate destruction of either chemical or biological weapons of mass destruction production facilities of both state and non-state actors. Both examples involve interaction of a blast with a container of material that can be either solid, liquid, or a mixture of both. These events can lead to the release of aerosol clouds that can carry hazardous material long distances, potentially exposing many people to toxic material. Specifically, the main objective of the present study is to construct a model which captures the essential physics of detonation and blast envelope growth, as well as subsequent atmospheric drag heating of the resulting fragments. The computed heating can be used to ascertain the survivability of small-scale biohazardous material contained within the blast fragments. For example, in many scenarios, heating can either kill microorganisms, chemically degrade chemicals, or create new, potentially hazardous, chemicals. It is thus essential to understand atmospheric heating.

---

* Corresponding author.
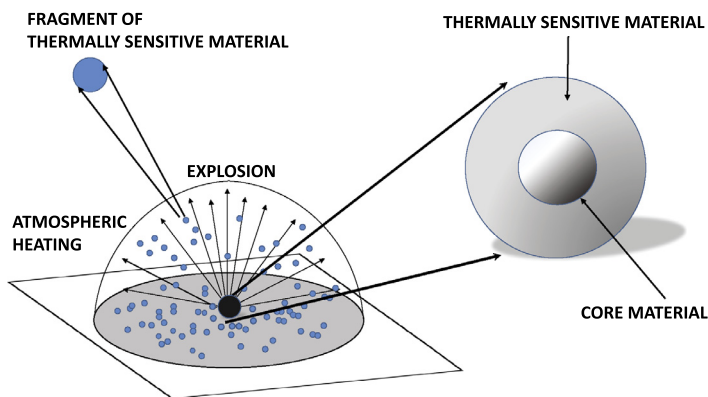 *E-mail address:* zohdi@me.berkeley.edu (T.I. Zohdi).

Fig. 1. Explosion of an object containing biomaterial experiencing atmospheric heating.

Fig. 2. Still frames from the field experiments.

As a model problem, we simulate an explosive device as a sphere that is hollowed out with an energetic material in the center (Fig. 1). The shell is extremely thin and is simply present to separate the inner core of explosives from the surrounding blast material which is to be tracked. In this work, we do not consider detailed models for the interaction between the shock wave and the packed fragments (see for example Cabalo, Schmidt, Wendt, & Scheeline, 2002; Gregoire, Sturtzer, & Khasainov, 2009; Hoover & Hoover, 2009; Kudryashova et al., 2011) nor the chemical aspects which are beyond the scope of the present work.

2. Motivation via experiments

The result from a set full scale field experiments with high explosives and ballistic gelatin motivates the desire to predict the dispersal of material by the blast as well as understand the effects of atmospheric heating. The primary conclusion that could be drawn from these experiments is that aerosols generated from a blast containing toxic materials cannot be assumed to be inactivated by the blast itself (Cabalo et al., 2016). For example, this result is in agreement with the findings of Eshkol and Katz (2005), and Kanemitsu (2005), where Hepatitis B was transmitted from a suicide bomber to survivors of the blast.

To summarize the set of experiments, we detonated blocks of ballistic gelatin with high explosives on a test range to explore the survivability of fragmented (particulate) material, as shown in Fig. 2. Ballistic gelatin was used in the test due to its well understood mechanical properties and relevance to previous human injury studies, and it is a thermally sensitive material that melts at approximately 40 °C. An aerosol particle sizer and a UV-fluorescent particle counter that was selectively sensitive to the protein of the ballistic gelatin monitored aerosols generated. A small amount of bacterial spores had been mixed into the gelatin, so that we could detect deposition of even very small amounts of material on witness plates. The use of living material also permitted an assessment of thermal damage to the material since temperatures in excess of 70 °C will kill the microorganisms. Although these experiments were far from quantitative, we could draw the conclusion that interaction of material with a detonation fireball was minimal, so that it cannot be assumed the detonation will consume the hazardous material. Although the ballistic gelatin we used melts at low temperatures in comparison to temperatures found in the blast, a large amount of solid gelatin was collected on the test pad. Furthermore, witness plates located approximately 100 m away from the blast site, collected aerosol fragments bearing viable organisms. These were detected by swabbing the witness plates with wetted wipes, and plating rinse onto agar plates. Bacterial colonies were then counted. Significant transient concentrations of aerosol (approximately 1000 particles/L) only attributable to the gelatin were detected. Again this means it cannot be assumed the heat and pressure from the blast will consume hazardous material, even if the proportion of high explosive to hazardous material is high.

The result of the test also highlighted the need for a good model. There are numerous possible configurations of containers of possible hazardous materials versus a blast, ranging from a large chemical tank to storage sites of weapons of
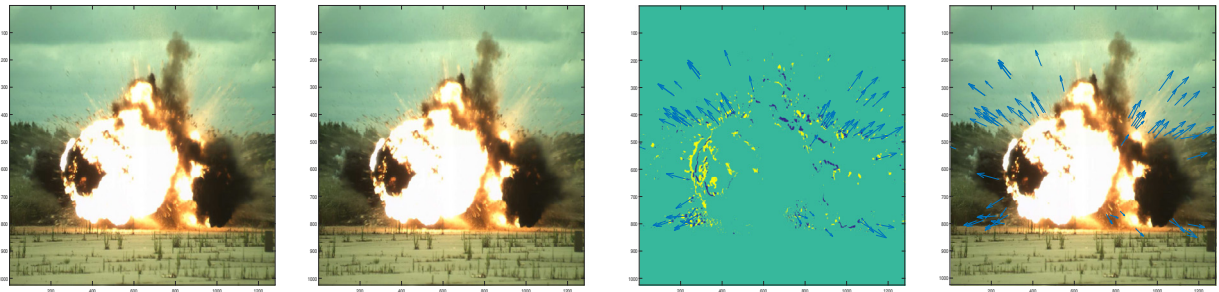
Fig. 3. The still frames(the first two panels (#1 and #2) are used to compute the object velocities in the panels #3 and #4).

mass destruction contained within 55 gallon drums destroyed by a munition. As a result, depending on the initial geometry, individual fragments ejected by the blast can experience greatly different thermal histories. The thermal history of each fragment will determine the amount of degradation or chemical change that that fragment will undergo. Thus, a good model of the atmospheric heating is essential for accurately predicting the resulting threat. Although the experiments briefly described above were not performed in a precisely controlled manner, high speed video of the detonation tests were recorded that provide fragment trajectory data for comparison between the model and experiment. Although transient thermal measurements were not recorded during the execution of the test, realistic trajectories of fragments were recorded to help validate the model.

2.1. Experiments

The objective of the analysis was to obtain an estimation of the footprint of material deposited by the blast that can be compared to the results of the modeling. Due to the use of a single high speed camera, our measurements of speed and direction were projections of the true velocity onto the image plane of the camera. Components of the velocity directed towards or away from the camera cannot be seen, and furthermore, perspective as a function of distance is not taken into account. However, we made the reasonable assumption that dispersion is isotropic (since it was a radially-outward blast), thus we need only determine the maximum distance objects will travel in one plane. We do not believe perspective in the image to be a problem because only objects within the image plane achieved the longest distance of travel and contribute to the footprint measurement. The maximum distances were used to compare to the model.

Because we used the high speed video from the experiments that provided the motivation for model development, we now provide additional experimental details. Experiments were performed at the test range at the Aberdeen Proving Ground. The test was performed for 3.6 kg TNT explosive (8 M1 Demolition Blocks) arranged around the 26.9 kg block of ballistic gelatin, sitting on a 120 cm tall platform (Fig. 2). Small amounts of fluorescent, food grade dye (WaterGlo 801, Spectroline, Inc.) were added to the gelatin (500 μL). High speed video was recorded at a safe distance from the detonation site at 100 m with a High Definition Olympus i-Speed 2 camera that has 1024×1280 pixels at a frame rate of 500 frames per second. Matlab 2016b was used to capture and analyze frames from the high speed video.

To determine velocities in the image plane of the camera, consecutive frames were used. We used pairs of frames primarily from 40 to 60 ms after the blast. Most objects were obscured in the earlier frames by the explosion flash, and yielded very high transient velocities that would not be sustained due to the effect of drag. Most objects had moved out of the camera view by later frames. Fig. 3, panels #1 − #4, demonstrate the analysis of the 8 pound TNT test. Objects of known dimensions in the scene were used to determine distances so that distances in pixels could be converted to physical distances. The difference image was taken of the two frames (Fig. 3, panels #1 and #2) by mathematically subtracting their pixel readings, and then converted to monochrome to simplify detection of objects in motion. Anything not in motion was eliminated from the image. A threshold filter was then applied to aid in the identification of individual objects. Moving objects appear twice in the image; once as an object with pixel values consisting of negative values, the second with positive pixel values. Shape and proximity of the two image components were used to uniquely identify objects in the difference image. The object centroids were used to determine position as well as the shift in position between frames. As a data check, the velocity vectors were superimposed over one of the unprocessed image frames as shown in Fig. 3, panel #4. We verified that the velocity vectors corresponded to real object images.

Not all objects gave two clean images that could be used to trace the velocity, so not every object visible in Fig. 3, panel #4, yielded a velocity vector. This occurred either because of contrast issues with the background, or the change in illumination from the explosion fireball. Nevertheless, a number of objects were tracked in each pair of images, allowing for determination of reasonable velocities and estimation of distance traveled. Velocities are determined by measuring the distance in pixels between an object's positive and negative images. Pixel distances were then converted to physical distance in the camera plane, and velocities were determined by the time difference (2 ms) between frames. We also used the velocity vector projected into the image plane to calculate distance traveled in that plane. To roughly calculate the airborne time of a fragment (after the initial frames of the explosion), we computed the time takes for an object to go up, starting at
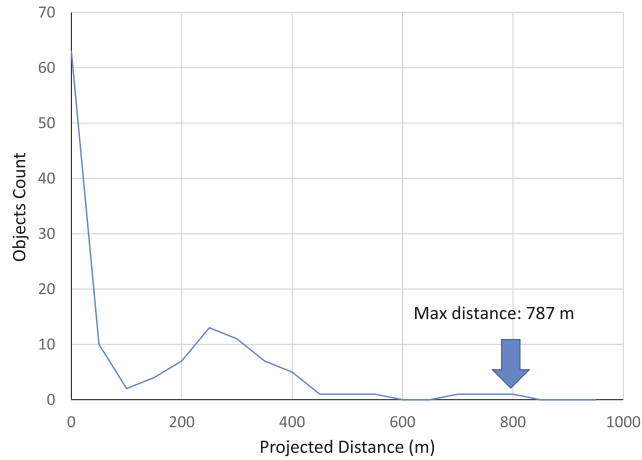
Fig. 4. Histogram of distance distributions.

a distance of h_o, with vertical component (v_{oy}) of the initial velocity $\boldsymbol{v}_o$ and then to come down from the maximum attained height (in free fall)

$$t_h = \underbrace{\frac{v_{oy}}{g}}_{\text{time up}} + \underbrace{\frac{1}{g}\sqrt{(v_{oy}^2 + 2gh_o)}}_{\text{time down}}. \tag{2.1}$$

To estimate the horizontal distance traveled of the fragment, we then multiplied t_h by the horizontal component of the velocity. To see the distribution of estimated deposition of objects as a function of distance from the test site, a histogram was generated from the video data. For each test size, a list of estimated object travel distances were generated. Object distances falling within the values of a bin produced a count within that bin, and all the counts in the bins were summed. The resulting histogram in Fig. 4 shows the distribution of distances traveled.

Remark: Because of the way we have experimentally estimated the initial velocity (v_o), from the initial frames in the preceding analysis, the drag has implicitly been accounted for, where it would be of the greatest effect. Beyond this initial stage, it is appropriate to comment on the implications of neglecting drag after the initial stages of the blast. First, it is not easy to directly estimate the drag effects analytically, since it is not constant (this will be discussed later in the paper). Drag will reduce the time to go up to the maximum height, however, it will increase the time it takes to come down. Thus, it is generally impossible to make a definitive analytical statement a priori on whether drag reduces or increases the distance travelled, thus motivating the analysis later in the paper.

2.2. Summary of the experimental results

The results are as follows:

- Fig. 3, panels #1 and #2, shows consecutive still frames from the test used to generate the difference image in panel #3. A fraction of the objects clearly appear twice in the difference image, and the distance between them is used to determine the velocity. Objects giving identifiable pairs of images are marked with a velocity vector in the difference image.
- Fig. 3, panel #4, shows still frame with velocity vectors superimposed. Each vector corresponds to a moving object that could be measured in the image.
- Fig. 4 shows a histogram of distance traveled. To calculate the histogram, the velocities of objects measured from the difference images(both speed and direction), were used to estimate distances traveled. Twenty 100 m interval bins were used up to 1000 m. A maximum distance of 787 m was obtained. From the video analysis we calculated an average speed of 56.1 m/s and a maximum of 119.6 m/s in the camera image plane.

A point to be made of detailed experiments is that they take an *inordinate amount of time* and it is impractical to do large numbers of parameter studies. Furthermore, the heating of the objects is difficult to ascertain. Both of these issues motivate the development of a rapid computational tool, which is the subject of this paper.

3. Simplifying assumptions for the computational model

We make the following simplifying assumptions:

- We will assume the same initial velocity for all fragments (based on our previous) camera observations, since the blasts under consideration are radially-outward (by construction). This of course naturally implies that a non-interaction approximation is appropriate. Specifically, the fragments do not interact with one another and are assumed spherical with radius R_i, $i = 1, 2, 3 \ldots N = fragments$. Based on the experimental observations, the blast fragments are quite small and for radially-outward blasts, the amount of rotation, if any, contributes negligibly (recall, the spherical shape of the charge and blast) to the overall trajectory of the fragments. We assume that upon detonation, each fragment has the same impulsive detonation velocity (denoted $\delta \boldsymbol{v}(0)$), in the radial direction from the center of the blast. The mass of the explosive material (TNT) is considered negligible and is converted to energy, which is imparted to the surrounding fragmenting material. The (polymeric) shell casing enclosing the explosive is extremely thin (essentially a plastic wrap) which is simply to hold the TNT together when placed within the gelatin. It plays no role in the subsequent explosion dynamics. Thus, mathematically, the velocity vector pulse is radially outward from the center of the sphere, co-located at the center of mass of the explosive material:

$$\delta \boldsymbol{v}_i(0) = ||\delta \boldsymbol{v}(0)|| \left(\frac{\boldsymbol{r}_i(0) - \boldsymbol{r}_c(0)}{||\boldsymbol{r}_i(0) - \boldsymbol{r}_c(0)||} \right) \overset{\text{def}}{=} ||\delta \boldsymbol{v}(0)|| \boldsymbol{n}_{ri} \tag{3.1}$$

where $\mathbf{r}_i$ is the position vector of the ith fragment, $\mathbf{n}_{ri}$ is the normal/radial direction and

$$\boldsymbol{r}_c(0) = \frac{1}{\left(\sum_{i=1}^{N} m_i \right)} \sum_{i=1}^{N} m_i \boldsymbol{r}_i(0), \tag{3.2}$$

where N is the number of fragments, $\mathbf{r}_c(0)$ is the center of mass of the fragmenting material and m_i is the mass of each fragment. In the general case where the object was moving before the blast, the pulse velocities are added to the velocity vectors immediately before the pulse ($\boldsymbol{v}^-(0)$)

$$\boldsymbol{v}_i^+(0) = \boldsymbol{v}_i^-(0) + \delta \boldsymbol{v}_i(0). \tag{3.3}$$

- The magnitude of the initial velocity pulse dictates initial energy released (E), which is assumed to be converted into kinetic energy for the material at ($t = 0$):

$$E = \sum_{i=1}^{N} \frac{1}{2} m_i ||\delta \boldsymbol{v}(0)||^2 \Rightarrow ||\delta \boldsymbol{v}(0)|| = \sqrt{\frac{2E}{\sum_{i=1}^{N} m_i}} = \sqrt{\frac{2E}{M}}, \tag{3.4}$$

where $\delta \boldsymbol{v}(0)$ is the velocity of pulse imparted to a fragment in the radial direction, M is the total detonation material mass, $m_i = \rho_i \frac{4}{3} \pi R_i^3$ is mass of the individual fragments, where ρ_i is the density of the fragments.
- For the objects, the effects of their rotation with respect to their mass center are unimportant to their overall motion. The equation of motion for the ith fragment in the system is

$$m_i \dot{\boldsymbol{v}}_i = \boldsymbol{\Psi}_i^{tot} = \boldsymbol{\Psi}_i^{drag} + \boldsymbol{\Psi}_i^{grav}, \tag{3.5}$$

with initial velocity $\boldsymbol{v}_i(0)$ and initial position $\mathbf{r}_i(0)$. The gravitational force is $\boldsymbol{\Psi}_i^{grav} = m_i \boldsymbol{g}$, where $\boldsymbol{g} = (g_x, g_y, g_z) = (0, 0, -9.81) \, m/s^2$.
- For the drag, we will employ a general phenomenological model

$$\boldsymbol{\Psi}_i^{drag} = \frac{1}{2} \rho_a C_D ||\boldsymbol{v}^f - \boldsymbol{v}_i|| (\boldsymbol{v}^f - \boldsymbol{v}_i) A_i, \tag{3.6}$$

where C_D is the drag coefficient, A_i is the reference area, which for a sphere is $A_i = \pi R_i^2$, ρ_a is the density of the ambient fluid environment and $\boldsymbol{v}^f$ is the velocity of the surrounding medium which, in the case of interest, is air.
- For the drag-heating rate, we take the inner-product of the drag force with the relative velocity of the fragment to the surrounding environment, and insert it into the First Law of Thermodynamics:

$$m_i C_i \dot{\theta} = \boldsymbol{\Psi}_i^{drag} \cdot (\boldsymbol{v}^f - \boldsymbol{v}_i) = \frac{1}{2} \rho_a C_D ||\boldsymbol{v}^f - \boldsymbol{v}_i|| (\boldsymbol{v}^f - \boldsymbol{v}_i) A_i \cdot (\boldsymbol{v}^f - \boldsymbol{v}_i) = \frac{1}{2} \rho_a C_D ||\boldsymbol{v}^f - \boldsymbol{v}_i||^3 A_i. \tag{3.7}$$

Remarks: For the problems under consideration, the non-interaction assumption is quite appropriate since all of the fragments are propagating radially outwards with the same initial velocity. Thus, the inter-fragment collisions are negligible. This has been repeated verified by "brute-force" collision calculations using formulations found in Zohdi (2013); 2014a). We will assume that the velocity of the surrounding medium ($\boldsymbol{v}^f$) is given, implicitly assuming that the dynamics of the surrounding medium are unaffected by the fragments.[1] We also remark that in the case of underwater blasts or fragments that become porous as a result of the blast ("fluffy"), a buoyancy force would need to be included, $\boldsymbol{\Psi}_i^{buoy} = \rho_f \frac{4}{3} \pi R_i^3 \boldsymbol{b}$, where $\boldsymbol{b} = (b_x, b_y, b_z) = (0, 0, 9.81) \, m/s^2$ and ρ_f is the density of the surrounding fluid. Neither of these cases are important in the present analysis, however, we refer the reader to Zohdi (2016).

---

[1] We will discuss this assumption later in the paper.

4. Approximate analytical solutions to special cases

4.1. Trajectories

If we assume that $\boldsymbol{v}^f \approx \boldsymbol{0}$, the differential equation for each fragment in its outward normal direction, assuming no gravity or fluid velocity ($\boldsymbol{v}^f = \boldsymbol{0}$)The subscript n indicates the outward normal direction.:

$$m_i \dot{v}_{in} = -\frac{1}{2}\rho_a C_D v_{in}^2 A_i, \tag{4.1}$$

where v_{in} is the outward normal velocity, which can be written as

$$\dot{v}_{in} = -K_i v_{in}^2, \tag{4.2}$$

where for a sphere

$$K_i = \frac{1}{2m_i} C_D \rho_a A_i = \frac{3C_D \rho_a}{8\rho R_i}. \tag{4.3}$$

Using the chain rule

$$\frac{dv_{in}}{dt} = \frac{dv_{in}}{dr_{in}}\frac{dr_{in}}{dt} = \frac{dv_{in}}{dr_{in}}v_{in} = -K_i v_{in}^2, \tag{4.4}$$

which yields

$$\frac{dv_{in}}{dr_{in}} = -Kv_{in}, \tag{4.5}$$

and subsequently

$$\frac{dv_{in}}{v_{in}} = -K dr_{in} \Rightarrow \int_{v_{oin}}^{v_{in}(t)} \frac{dv_{in}}{v_{in}} = -\int_{r_{oin}}^{r_{in}(t)} K dr_{in}, \tag{4.6}$$

where r_{in} is the outward normal position, with solution

$$v_{in}(t) = v_{oin} e^{-K(r_{in}(t) - r_{oin})}, \tag{4.7}$$

with inverse solution, for the blast radius

$$\mathcal{L}(t) = r_{in}(t) - r_{oin} = -\frac{1}{K} Ln\left(\frac{v_{in}(t)}{v_{oin}}\right) = -\frac{8\rho R_i}{3C_D \rho_a} Ln\left(\frac{v_{in}(t)}{v_{oin}}\right), \tag{4.8}$$

where $\frac{1}{K}$ has units of meters. This shows the explict inverse relationship between the size of the blast radius and K, which is a measure of the drag (tending to limit the blast radius growth) and the mass (tending to increase the blast radius growth). One can relate this directly to the energy of detonation and total mass via Eq. (3.4), utilizing $v_{oin} = \sqrt{\frac{2E}{M}}$

$$\mathcal{L}(t) = r_{in}(t) - r_{oin} = -\frac{8\rho R_i}{3C_D \rho_a} Ln\left(\frac{v_{in}(t)}{\sqrt{\frac{2E}{M}}}\right). \tag{4.9}$$

Remark: One could directly integrate Eq. (4.2) in time to yield

$$v_{in}(t) = \frac{v_{oin}}{K t v_{oin} + 1} = \frac{\sqrt{\frac{2E}{M}}}{K t \sqrt{\frac{2E}{M}} + 1} \tag{4.10}$$

and

$$r_{in}(t) = r_{oin} + \frac{1}{K} Ln(K_i t_i v_{oin} + 1) = r_{oin} + \frac{1}{K_i} Ln\left(K_i t_i \sqrt{\frac{2E}{M}} + 1\right). \tag{4.11}$$

One can also invert Eq. (4.11) to yield an expression for the time it takes to achieve a certain blast radius:

$$t_i^* = \frac{e^{K_i(r_{in}(t) - r_{oin})} - 1}{K_i \sqrt{\frac{2E}{M}}}. \tag{4.12}$$

4.2. Atmospheric heating

The atmospheric heating of the material is given by Eq. (3.7) which, in the general case, can be integrated to yield:

$$\theta(t) = \theta(t = 0) + \frac{1}{m_i C_i} \int_0^t \boldsymbol{\Psi}_i^{drag} \cdot (\boldsymbol{v}^f - \boldsymbol{v}_i) \, dt, \tag{4.13}$$

where

$$\int_0^t \boldsymbol{\Psi}_i^{drag} \cdot (\boldsymbol{v}^f - \boldsymbol{v}_i) \, dt = \int_0^t \frac{1}{2} \rho_a C_D ||\boldsymbol{v}^f - \boldsymbol{v}_i||^3 A_i \, dt, \tag{4.14}$$

which shows a cubic-dependency on the relative velocity. In the special case considered in the previous section,

$$||\boldsymbol{v}^f - \boldsymbol{v}_i||^3 = \left(\frac{v_{oin}}{K_i t v_{oin} + 1} \right)^3 = \left(\frac{\sqrt{\frac{2E}{M}}}{K_i t \sqrt{\frac{2E}{M}} + 1} \right)^3, \tag{4.15}$$

or, explicitly,

$$\theta_i(t) = \theta_i(t = 0) + \frac{1}{m_i C_i} \int_0^t \frac{1}{2} \rho_a C_D \left(\frac{\sqrt{\frac{2E}{M}}}{K_i t \sqrt{\frac{2E}{M}} + 1} \right)^3 A_i \, dt. \tag{4.16}$$

5. More accurate resolution of drag

To more accurately account for the effects of drag, one must take into account that the empirical drag coefficient varies with Reynolds number. For example, consider the following piecewise relation (Chow, 1980):

- For $0 < Re \leq 1$, $C_D = \frac{24}{Re}$,
- For $1 < Re \leq 400$, $C_D = \frac{24}{Re^{0.646}}$,
- For $400 < Re \leq 3 \times 10^5$, $C_D = 0.5$,
- For $3 \times 10^5 < Re \leq 2 \times 10^6$, $C_D = 0.000366 Re^{0.4275}$,
- For $2 \times 10^6 < Re < \infty$, $C_D = 0.18$,

where the local Reynolds number for a fragment is $Re \overset{\text{def}}{=} \frac{2R\rho_a||\boldsymbol{v}^f - \boldsymbol{v}_i||}{\mu_f}$ and μ_f is the fluid viscosity.[2] We note that in the zero Reynolds number limit the drag is Stokesian. Using the piecewise relation reduces the drag at the lower Reynolds number regimes, thus producing a larger blast radius than a constant large drag coefficient. The governing equation, when include gravity is included, is

$$m_i \dot{\boldsymbol{v}}_i = \boldsymbol{\Psi}_i^{drag} + \boldsymbol{\Psi}_i^{grav} = \frac{1}{2} \rho_a C_D ||\boldsymbol{v}^f - \boldsymbol{v}_i||(\boldsymbol{v}^f - \boldsymbol{v}_i) A_i + m_i \boldsymbol{g}, \tag{5.1}$$

which we must integrate the governing equations numerically

$$\begin{aligned} \boldsymbol{v}_i(t + \Delta t) &= \boldsymbol{v}_i(t) + \frac{1}{m} \int_t^{t+\Delta t} (\boldsymbol{\Psi}_i^{drag} + \boldsymbol{\Psi}_i^{grav}) \, dt \\ &\approx \boldsymbol{v}_i(t) + \frac{\Delta t}{m_i} \left(\boldsymbol{\Psi}_i^{drag}(t) + \boldsymbol{\Psi}_i^{grav}(t) \right). \end{aligned} \tag{5.2}$$

We can subsequently integrate for the temperature

$$\theta_i(t + \Delta t) = \theta_i(t) + \frac{1}{m_i C_i} \int_t^{t+\Delta t} \frac{1}{2} \rho_a C_D ||\boldsymbol{v}^f - \boldsymbol{v}_i||^3 A \, dt = \theta_i(t) + \frac{\Delta t \rho_a C_D A_i}{2 m_i C_i} ||\boldsymbol{v}^f - \boldsymbol{v}_i(t)||^3. \tag{5.3}$$

Remark: The piecewise drag law of Chow (1980) is a mathematical description for the Reynolds number over a wide range and is a curve-fit of extensive data from Schlichtling (1979). As observed in the experimental data, the mathematical function exhibits a discontinuity at $Re = 3 \times 10^5$, although in an explosion the time a fragment resides in this Reynolds number is negligible.

6. Numerical examples

In order to illustrate the model, the following simulation parameters were chosen:

- Total simulation duration, 20 s,
- The time step size, $\Delta t = 10^{-4}$ s,

---

[2] The viscosity coefficient for air is $\mu_f = 0.000018$ Pa/s.

- Launch velocity, $\boldsymbol{v}(t = 0) = (0, 0, 0)$ m/s (no obstructions),
- Detonation energy, $E = 3.61$ kg TNT or $E = 16.66 \times 10^6$ J (TNT=4.6 $\times 10^6$ J/kg),
- Density of air, $\rho_a = 1.225$ kg/m^3,
- Number of fragments, $N = 1000$,
- Density of detonation material, $\rho = 1000$ kg/m^3,
- Total mass, $M = \sum_{i=1}^{N} m_i = 26.15$ kg and
- Heat capacity of $C = 1900$ J/K – kg.

The fragment sizes were randomly generated and scaled so that the total mass in the system remains constant and ere packed between the inner and outer shell cited above. We assumed that the TNT was converted into an energy impulse to the mass of the gelatin. An extremely small (relative to the total simulation time) time-step size of $\Delta t = 10^{-4}$ s was used. Further reductions of the time-step size produced no noticeable changes in the results, thus the solutions generated can be considered to have negligible numerical error. The simulations took under 1 min on a standard laptop. Fig. 5 illustrates the results for the parameters above. With the chosen parameters, with ground constraints (starting at 1 m high):

- Case 1: With uniform sized fragment masses, $m_i = M/N$ with detonation energy, $E = 3.6$ kg TNT $E = 16.66 \times 10^6$ J, with mass of 26.15 kg yielded a maximum blast radius of 596.278 m (farthest traveling object) and a mean temperature of $\theta = 174.87$ K. However, as Fig. 5 clearly indicates material at the core that hits the ground has minimal temperature rise near the blast. The maximum temperature is approximate 615 K.
- Case 2: With random sized fragment masses, $m_i = (M/N)(1 + A_i)$, where $-0.95 \leq A_i \leq 0.95$, with detonation energy, $E = 3.6$ kg TNT $E = 16.66 \times 10^6$ J, with mass of 26.15 kg yielded a maximum blast radius of 784.920 m (farthest traveling object) and a mean temperature of $\theta = 174.34$ K. However, as Fig. 6 clearly indicates material at the core that hits the ground has minimal temperature rise near the blast. The maximum temperature is approximate 615 K.

The randomized fragment case matched quite closely with the experiments in terms of the blast radius. We clearly see that the fragments that travel further, they are heated more. The fragments that stop closer have been heated less and *potentially are still contaminants*, i.e. the material has not been heated sufficiently, and the location in which it lands can be considered as "contaminated/hazardous". We note that in the descending phase of the trajectory, the fragments nearly achieve a so-called settling steady-state velocity, v_{tm} (when $\dot{\boldsymbol{v}} = \mathbf{0}$), given by assuming a purely vertical trajectory drop

$$m\dot{v} = m\boldsymbol{g} + m_a \boldsymbol{b} + \frac{1}{2}\rho_a A C_D \boldsymbol{v}||\boldsymbol{v}|| \Rightarrow 0 = -mg + m_a g + \frac{1}{2}\rho_a A C_D v_{tm}^2 \Rightarrow v_{tm} = \sqrt{\frac{2(m - m_a)g}{\rho_a C_D A}}, \tag{6.1}$$

where an implicit equation for the settling velocity arises due to the drag coefficient's dependency on $C_D(v)$.

Remark: In the low velocity (low Reynolds number) limit a Stokesian model is most appropriate, which is what the drag law above attempts to incorporate. The drag forces are significantly smaller with a Stokesian model. Comparing a purely Stokesian drag law, which would be valid for small fragments and laminar flow (low Reynolds number)

$$\boldsymbol{\Psi}_i^{drag,Stokesian} = c(\boldsymbol{v}^f - \boldsymbol{v}_i) = \mu_f 6\pi R_i (\boldsymbol{v}^f - \boldsymbol{v}_i), \tag{6.2}$$

where μ_f is the fluid viscosity. We observe the following:

$$\frac{||\boldsymbol{\Psi}^{drag,Stokesian}||}{||\boldsymbol{\Psi}^{drag}||} = \frac{12\mu_f}{\rho_a C_D R||\boldsymbol{v}^f - \boldsymbol{v}_i||}. \tag{6.3}$$

For typical parameters for air and spherical fragments (using $C_D = 0.5$, which is a mid-range value from the piecewise drag law introduced earlier), we have

$$\frac{||\boldsymbol{\Psi}^{drag,Stokesian}||}{||\boldsymbol{\Psi}^{drag}||} = \frac{12\mu_f}{\rho_a C_D R||\boldsymbol{v}^f - \boldsymbol{v}_i||} \approx \frac{0.0004}{R||\boldsymbol{v}^f - \boldsymbol{v}_i||}, \tag{6.4}$$

which indicates that for extremely small fragments and low velocities, the Stokesian model dominates, while for larger fragments and large velocities, the phenomenological model dominates.

7. Summary

The comparison of the example calculation from the model and the high speed video analysis from our field tests show the reasonableness of the model. The maximum distance for an object hurled by the blast as determined from the video matched closely to the predicted distances for the model for randomly sized fragments (787 m versus 784.92 m, respectively). A smaller radius is obtained for the case of uniform spheres (596.278 m), but this is to be expected given the absence of larger fragments in this simulation that are less affected by drag. We attempted to scale the model down to match smaller scale field tests, but found a limit with respect to simulation size. Smaller systems led to too few fragments for good statistics with the model. The use of uniform or randomly sized fragments did not much affect the predicted average or maximum temperature. We expect to validate the temperature aspect of the model with thermal imaging of future tests.
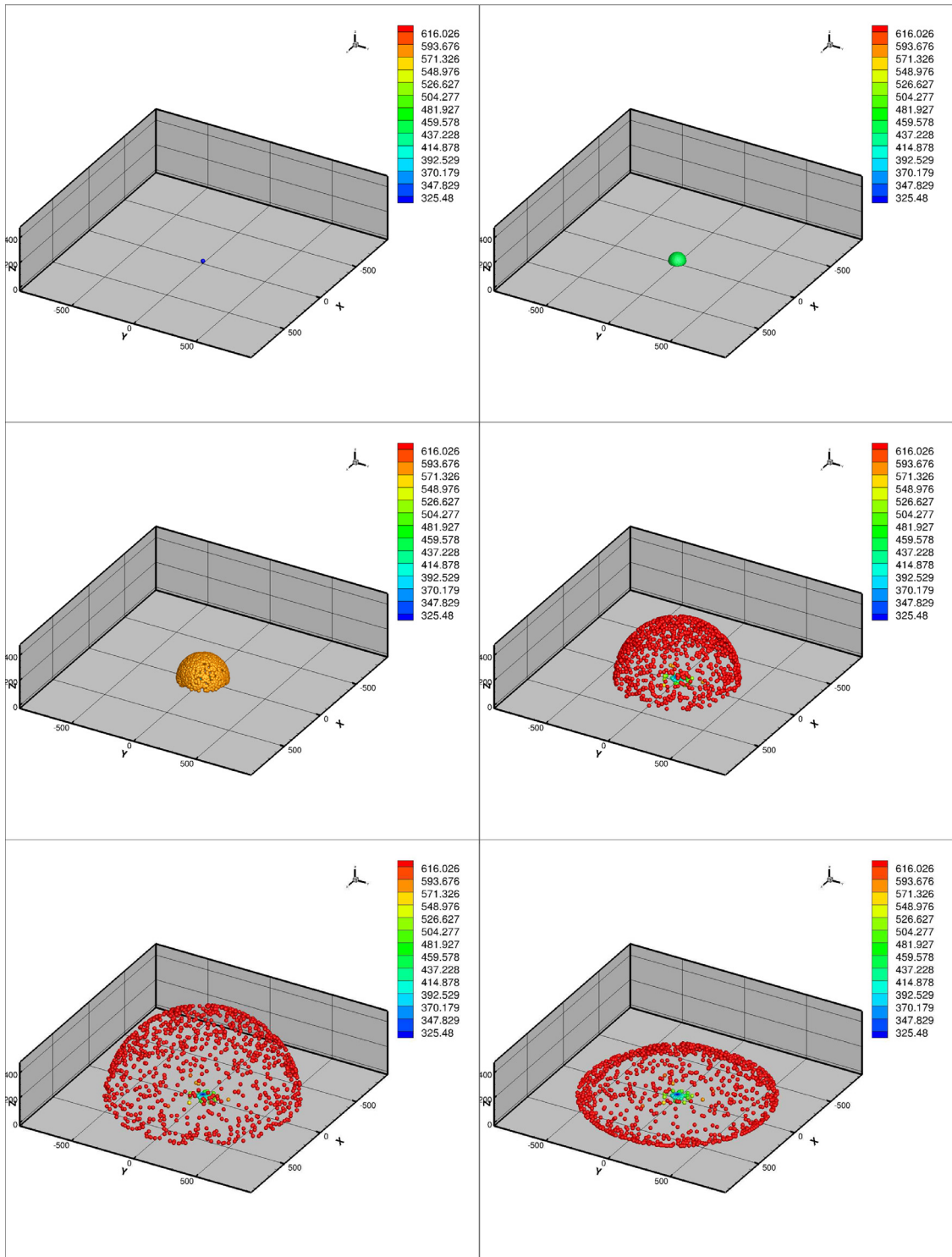
Fig. 5. Case 1: With uniform fragment masses, $m_i = M/N$. Detonation energy, $E = 3.6$ kg TNT $E = 16.66 \times 10^6$ J, with mass of 26.15 kg yielded a blast radius of 596.278 m and a mean temperature of $\theta = 174.87$ K. However, as the Figure clearly indicates material at the core that hits the ground has minimal temperature rise near the blast. The maximum temperature is approximate 615 K.
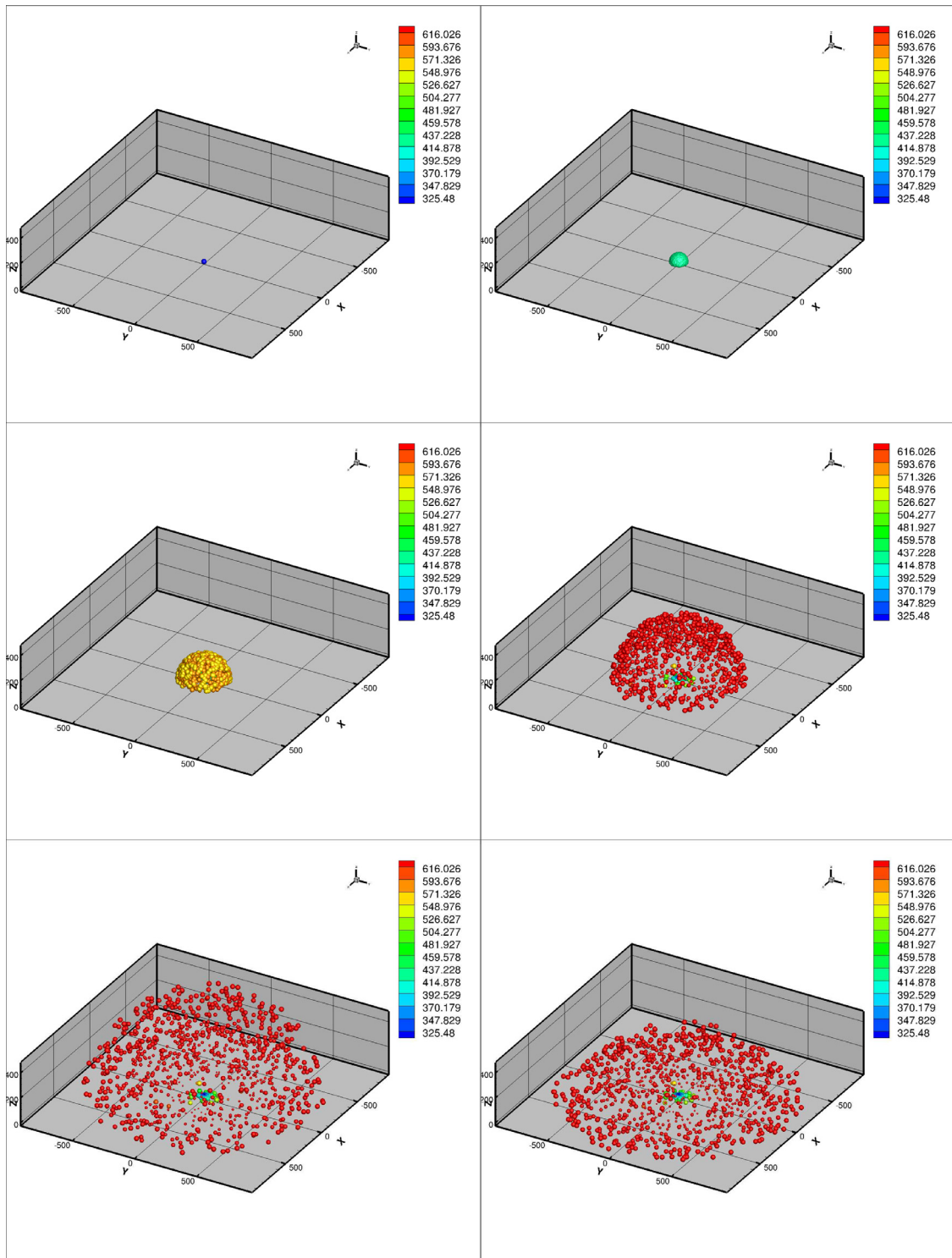
Fig. 6. Case 2: With random fragment masses, $m_i = (M/N)(1 + A_i)$, where $-0.95 \leq A_i \leq 0.95$, with detonation energy, $E = 3.6$ kg TNT $E = 16.66 \times 10^6$ J, with mass of 26.15 kg yielded a blast radius of 784.920 m and a mean temperature of $\theta = 174.34$ K. However, as Fig. 6 clearly indicates material at the core that hits the ground has minimal temperature rise near the blast. The maximum temperature is approximate 615 K. We note that for the case of random fragment masses, we obtained a larger radius for the fragment footprint. We attribute this to more massive fragments are created that are less affected by drag. As a result, a fraction of these fragments travel further. Although this observation could lead to the conclusion that the high drag experienced by aerosol particles would limit their dispersion, these can travel even longer distances. This is possible because aerosols have slow settling velocities and remain suspended for long periods of time. The long suspension times allow them to be carried long distances by ambient wind.

For general blast conditions, there can be cases where the change in the surrounding fluid's behavior, due to the motion of the fragments, may be important. For example, this entails numerically integrating the governing equations, which leads to (for example using a trapezoidal rule with variable integration metric, $0 \leq \phi \leq 1$)

$$
\begin{aligned}
\boldsymbol{v}_i(t + \Delta t) &= \boldsymbol{v}_i(t) + \frac{1}{m_i} \int_t^{t+\Delta t} \left(\boldsymbol{\Psi}_i^{grav} + \sum_{j=1, j\neq i}^{K} \boldsymbol{\Psi}_{ij} + \boldsymbol{\Psi}_i^{fluid} \right) dt \\
&\approx \boldsymbol{v}_i(t) + \frac{\Delta t \phi}{m_i} \left(\boldsymbol{\Psi}_i^{grav}(t + \Delta t) + \sum_{j=1, j\neq i}^{K} \boldsymbol{\Psi}_{ij}(t + \Delta t) + \boldsymbol{\Psi}_i^{fluid}(t + \Delta t) \right) \\
&+ \frac{\Delta t (1 - \phi)}{m_i} \left(\boldsymbol{\Psi}_i^{grav}(t) + \sum_{j=1, j\neq i}^{N} \boldsymbol{\Psi}_{ij}(t) + \boldsymbol{\Psi}_i^{fluid}(t) \right),
\end{aligned}
\tag{7.1}
$$

where $\boldsymbol{\Psi}_i^{fluid}$ represents the interaction of fragment i with the fluid and $\boldsymbol{\Psi}_{ij}(t)$ represents its interaction with the neighboring $j = 1, 2, \ldots N$ fragments. The position can be computed via application of the trapezoidal rule again:

$$
\boldsymbol{r}_i(t + \Delta t) \approx \boldsymbol{r}_i(t) + \Delta t (\phi \boldsymbol{v}_i(t + \Delta t) + (1 - \phi) \boldsymbol{v}_i(t)),
\tag{7.2}
$$

which can be consolidated into

$$
\begin{aligned}
\boldsymbol{r}_i(t + \Delta t) &= \boldsymbol{r}_i(t) + \boldsymbol{v}_i(t) \Delta t \\
&+ \frac{\phi^2 (\Delta t)^2}{m_i} \left(\boldsymbol{\Psi}_i^{grav}(t + \Delta t) + \sum_{j=1, j\neq i}^{N} \boldsymbol{\Psi}_{ij}(t + \Delta t) + \boldsymbol{\Psi}_i^{fluid}(t + \Delta t) \right) \\
&+ \frac{\phi (1 - \phi)(\Delta t)^2}{m_i} \left(\boldsymbol{\Psi}_i^{grav}(t) + \sum_{j=1, j\neq i}^{K} \boldsymbol{\Psi}_{ij}(t) + \boldsymbol{\Psi}_i^{fluid}(t) \right).
\end{aligned}
\tag{7.3}
$$

Also, for the thermal components:

$$
\begin{aligned}
\theta_i(t + \Delta t) &= \theta_i(t) + \frac{1}{m_i C_i} \int_t^{t+\Delta t} \frac{1}{2} \rho_a C_D ||\boldsymbol{v}^f - \boldsymbol{v}_i||^3 A \, dt \\
&= \theta_i(t) + \frac{\Delta t \rho_a C_D A_i}{2 m_i C_i} \left(\phi ||\boldsymbol{v}^f(t + \Delta t) - \boldsymbol{v}_i(t + \Delta t)||^3 + (1 - \phi) ||\boldsymbol{v}^f(t) - \boldsymbol{v}_i(t)||^3 \right).
\end{aligned}
\tag{7.4}
$$

The result is a system of coupled equations between the fragments and the fluid, requiring spatio-temporal discretization employing a possible combination of Discrete Element Methods with Finite Element or Finite Difference Methods. For example see Avci and Wriggers (2012), Bolintineanu et al. (2014), Leonardi, Wittel, Mendoza, and Herrmann (2014), Onate, Celigueta, Idelsohn, Salazar, and Surez (2011), Onate et al. (2014) and Onate, Idelsohn, Celigueta, and Rossi (2008), Zohdi (2004), Zohdi (2007; 2010; 2013; 2014a; 2014b). This is currently being pursued by the authors.

In closing, we present a simple blast dispersion model that is in qualitative agreement with field tests in terms of the radius of the footprint of deposited material. Yet, our field tests demonstrate the presence of aerosols of concern. The authors are also pursuing the expansion of this model using discrete particle methods to include aerosol source terms. These source terms are applicable to atmospheric transport models that can predict long range transport.

References

Avci, B., & Wriggers, P. (2012). A DEM-FEM coupling approach for the direct numerical simulation of 3D particulate flows. *Journal of Applied Mechanics, 79*. 010901-(1–7).

Bolintineanu, D. S., Grest, G. S., Lechman, J. B., Pierce, F., Plimpton, S. J., & Schunk, P. R. (2014). Particle dynamics modeling methods for colloid suspensions. *Computational Particle Mechanics, 1*(3), 321–356.

Cabalo, J., Schmidt, J., Wendt, J. O. L., & Scheeline, A. (2002). Spectrometric system for characterizing drop and powder trajectories and chemistry in reactive. *Flows Applied Spectroscopy, 56*, 1346–1353.

Cabalo, J. B., Kesavan, J., Sickenberger, D. W., Diviacchi, G., Maldonado-Figueroa, C., McGrady, D., & Stafford, K. (2016). Assessing the biological threat posed by suicide bombers. Report ECBC-TR-1363.

Chow, C. Y. (1980). *An introduction to computational fluid dynamics*. New York: Wiley.

Eshkol, Z., & Katz, K. (2005). Injuries from biologic material of suicide bombers. *Injury, 36*, 271–274.

Gregoire, Y., Sturtzer, M.-O., Khasainov, B. A., & Veyssiere, b. (2009). *Investigation of the behavior of solid particles dispersed by high explosive*. ICT 40th, 35/1–35/12.

Hoover, W. G., & Hoover, C. G. (2009). Tensor temperature and shock-wave stability in a strong two-dimensional shock wave. *Physical Reviews E: Statistical, Nonlinear, Soft Matter Physics, 80*. 011128/1-011128/6.

Kanemitsu, K., et al. (2005). Does incineration turn infectious waste aseptic? *Journal of Hospital Infection, 60*(4), 304–306.

Kudryashova, O. B., Vorozhtsov, B. I., Muravlev, E. V., Akhmadeev, I. R., Pavlenko, A. A., & Titov, S. S. (2011). Physicomathematical modeling of explosive dispersion of liquid and powders. *Propellants, Explosives, Pyrotechnics, 36*, 524–530.

Leonardi, A., Wittel, F. K., Mendoza, M., & Herrmann, H. J. (2014). Coupled DEM-LBM method for the free-surface simulation of heterogeneous suspensions. *Computational Particle Mechanics, 1*(1), 3–13.

Onate, E., Celigueta, M. A., Idelsohn, S. R., Salazar, F., & Surez, B. (2011). Possibilities of the particle finite element method for fluid-soil-structure interaction problems. *Computational Mechanics, 48*, 307–318.

Onate, E., Celigueta, M. A., Latorre, S., Casas, G., Rossi, R., & Rojek, J. (2014). Lagrangian analysis of multiscale particulate flows with the particle finite element method. *Computational Particle Mechanics, 1*(1), 85–102.

Onate, E., Idelsohn, S. R., Celigueta, M. A., & Rossi, R. (2008). Advances in the particle finite element method for the analysis of fluid-multibody interaction and bed erosion in free surface flows. *Computer Methods in Applied Mechanics and Engineering, 197*(19–20), 1777–1800.

Schlichtling, H. (1979). *Boundary-layer theory* (7th ed.). New York: McGraw-Hill.

Zohdi, T. I. (2004). A computational framework for agglomeration in thermo-chemically reacting granular flows. In *Proceedings of the Royal Society. Vol. 460. Num. 2052* (pp. 3421–3445).

Zohdi, T. I. (2007). Computation of strongly coupled multifield interaction in particle-fluid systems. *Computer Methods in Applied Mechanics and Engineering, 196*, 3927–3950.

Zohdi, T. I. (2010). On the dynamics of charged electromagnetic particulate jets. *Archives of Computational Methods in Engineering, 17*(2), 109–135.

Zohdi, T. I. (2013). Numerical simulation of charged particulate cluster-droplet impact on electrified surfaces. *Journal of Computational Physics, 233*, 509–526.

Zohdi, T. I. (2014a). Additive particle deposition and selective laser processing-a computational manufacturing framework. *Computational Mechanics, 54*, 171–191.

Zohdi, T. I. (2014b). Mechanically-driven accumulation of microscale material at coupled solid-fluid interfaces in biological channels. *Proceedings of the Royal Society Interface, 11*, 20130922.

Zohdi, T. I. (2016). A note on firework blasts and qualitative parameter dependency. *Proceedings of the Royal Society*. doi:10.1098/rspa.2015.0720.